

Modeling the residual circulation of a coastal embayment affected by wind-driven upwelling: Circulation of the Ría de Vigo (NW Spain)

C. Souto

Facultad de Ciencias, Universidad de Vigo, Vigo, Spain

M. Gilcoto

Instituto de Investigacións Mariñas, Vigo, Spain

L. Fariña-Busto

Facultad de Ciencias, Universidad de Vigo, Vigo, Spain

Fiz. F. Pérez

Instituto de Investigacións Mariñas, Vigo, Spain

Received 12 June 2002; revised 24 June 2003; accepted 23 July 2003; published 5 November 2003.

[1] The barotropic and baroclinic nontidal circulations of the Ría de Vigo (NW Spain) are studied using the three-dimensional finite difference model HAMSOM (Hamburg Shelf Ocean Model). The external forcing acting on the system includes winds, freshwater inflow in the inner part of the ria and all over its surface, and heat exchange with the atmosphere. Modeled velocity is compared with data from an AANDERAA DCM12 acoustic Doppler current meter at one site of the ria, and predicted salinity and temperature fields contrasted with SEABIRD conductivity-temperature-depth data along the main channel of the ria. All predicted current, salinity, and temperature fields are in good agreement with experimental data. A new residual circulation pattern of the Ría de Vigo and its dependence on coastal winds is described. According to this pattern the typical estuarine two-layer circulation overlays in the outer part of the ria with a lateral circulation, resulting in a three-dimensional dynamics. The lateral circulation is induced by interaction between the southward (northward) alongshore coastal jet associated with upwelling (downwelling) winds and the topographic configuration of the ria. *INDEX*

TERMS: 4512 Oceanography: Physical: Currents; 4255 Oceanography: General: Numerical modeling; 4235 Oceanography: General: Estuarine processes; 4279 Oceanography: General: Upwelling and convergences; 4219 Oceanography: General: Continental shelf processes; 4536 Oceanography: Physical: Hydrography; *KEYWORDS:* currents, finite difference model, estuaries, Ría de Vigo (NW Spain)

Citation: Souto, C., M. Gilcoto, L. Fariña-Busto, and F. F. Pérez, Modeling the residual circulation of a coastal embayment affected by wind-driven upwelling: Circulation of the Ría de Vigo (NW Spain), *J. Geophys. Res.*, 108(C11), 3340, doi:10.1029/2002JC001512, 2003.

1. Introduction

[2] The Rías Baixas (latitude $42^{\circ}15'N$, longitude $8^{\circ}50'W$) are four coastal embayments located south of Cape Fisterra (Figure 1), along the northwest Atlantic coast of the Iberian Peninsula. The Rías Baixas are geographically and geomorphologically classified as rias [Cotton, 1956] and usually have been thermohaline and dynamically classified as partially mixed estuaries [Fraga and Margalef, 1979; Prego *et al.*, 1990] though, recently, Alvarez-Salgado *et al.* [2000] have argued for classifying them “like” estuaries not “as” estuaries. The southernmost of them is mesotidal and partially mixed Ría de Vigo (Figure 1), which extends

32 km, broadening steadily in a NE-SW direction, from 1 km width in its inner part (NE), at Rande Strait, to 10 km at the mouth of the ria (SW). It deepens as one moves to the outer region, ranging along the channel of the ria from maximum depths of 20 m in Rande Strait to 40–50 m in the southwestern side. The connection of the ria with the shelf is separated in two mouths by the Cíes Islands. The northern mouth is 2.5 km wide and has a maximum depth of 25 m. The southern one is 5 km wide, 50 m deep, and has a section four times larger than the northern one. The ria covers a total surface of 156 km^2 with a total volume of $3 \times 10^9 \text{ m}^3$. Eastward of Rande Strait is “San Simón Bay,” a very shallow area with an average depth of 3 m, which collects most of the continental water input to the ria. The most important freshwater inflow to the ria is the Oitaben-Verdugo River, whose waters reach the ria after flowing into the San

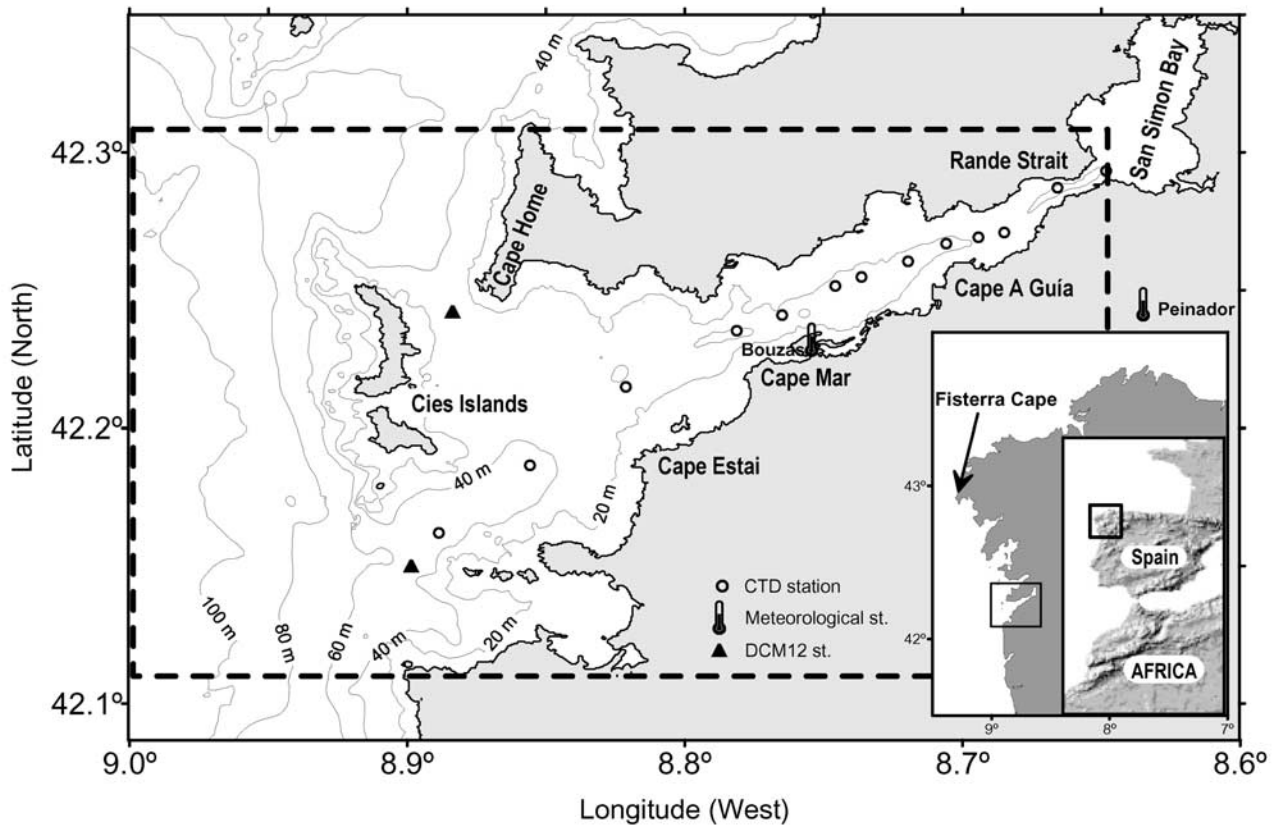


Figure 1. The Ría de Vigo. The open circles show the position of the CTD stations located over the main channel. The solid triangles in the north and south mouth correspond to the moorings of AANDERAA DCM12 Doppler current meters. The square drawn with a dashed line delimits the domain where the HAMSOM model was applied. The meteorological observatories at Cape Fisterra, Peinador airport, and Bouzas are also indicated.

Simón Bay. Together, Oitaben and Verdugo Rivers produce an annual mean freshwater flux of $13 \text{ m}^3 \text{ s}^{-1}$, ranging from about $5 \text{ m}^3 \text{ s}^{-1}$ in summer up to $120 \text{ m}^3 \text{ s}^{-1}$ in winter.

[3] The western coast of the Iberian Peninsula, where the rías Baixas are located (Figure 1), is the northern boundary of the NW Africa coastal upwelling system. At these latitudes (37° – 43°N) shelf winds follow a seasonal pattern associated to the large-scale climatology of the NE Atlantic. Upwelling-favorable northerly winds are predominant from March–April to September–October, while downwelling-favorable southerly winds predominate the rest of the year [Wooster *et al.*, 1976; McClain *et al.*, 1986; Blanton *et al.*, 1994]. The cold and nutrient-rich Eastern North Atlantic Central Water (ENACW) is promoted to the shelf during the upwelling period [Fraga, 1981; Fiuza, 1983], while warm and salty surface waters of subtropical origin piles on the shelf during the downwelling period [Frouin *et al.*, 1990; Haynes and Barton, 1990, 1991]. The upwelling, downwelling, and the transitions among them are, from a chemical and biological point of view, well-known short time events (2–4 days) that affect the residual circulation of the Rías Baixas [Álvarez-Salgado *et al.*, 2000; Gilcoto *et al.*, 2001]. These processes are very important because the Rías Baixas are among the more productive oceanic regions of the world [Blanton *et al.*, 1984], e.g., mean annual values of net primary production in the Ría de Vigo are about

$800 \text{ mg C m}^{-2} \text{ d}^{-1}$ [Prego, 1993] with maxima values up to $1800 \text{ mg C m}^{-2} \text{ d}^{-1}$ [Vives and Fraga, 1961] and have been related with human activities of economic interest as the mussel production [Blanton *et al.*, 1987]. So although in terms of energy the tide is one of the main driving forces affecting the Ría de Vigo and the river discharge favors a positive estuarine circulation, the wind stress and the shelf-ria interaction cannot be forgotten when studying the residual circulation of the ria.

[4] Since Ianniello [1977], the influence of the tide in the residual currents of estuaries has been extensively studied. Studies range from the behavior of the tide with different channel shapes [Ianniello, 1979; Jay, 1991; Li and O'Donnell, 1997; Li and Valle-Levinson, 1999] to the link between tides and stratification [Jay and Smith, 1990a, 1990b; Stacey *et al.*, 1999; Simpson *et al.*, 1990]. Examples of river influence in estuarine residual circulation are also more or less well spread in the literature of the past few years [Garvine *et al.*, 1992; Peters, 1997; Jay and Flinchem, 1997; MacCready, 1998], and obviously it is behind the classical salt balance proposed by Pritchard [1954] and the similarity solution of Rattray and Hansen [1962]. However, many times in the Ría de Vigo the main driving force that modulates the residual circulation is the wind, not only the local wind inside the ria but just the shelf wind and the associated Ekman transport. The wind-driven shelf

[Csanady, 1982] and estuarine circulation [Dyer, 1997] have also been the aim of many articles, but the key question is the relation between upwelling and residual circulation. There are several examples of the remote wind influence in estuaries cited by Wong and Moses-Hall [1998], and Garvine [1985] and Masse [1990] have faced the problem theoretically. In the present paper, and with the aid of a numerical model (the Hamburg Shelf Ocean Model (HAMSOM) model) and field current meter data, examples of residual current controlled by upwelling events will be introduced in order to show this mechanism in the Ría de Vigo. This fact will corroborate the information that box models [Rosón *et al.*, 1997; Álvarez-Salgado *et al.*, 2000; Pardo *et al.*, 2001] have revealed in the past about the Rías Baixas residual circulation. Once the direct relation that connects upwelling with the residual circulation is established in the Ría de Vigo, it is possible to adventure a pattern of low-frequency ($<1 \text{ d}^{-1}$) circulation in the Region of Freshwater Influence (ROFI) [Simpson, 1997], composed of the Ría de Vigo and the adjacent shelf.

[5] After description of the materials (section 2.1) and the model (section 2.2) used in this work, including the explanation of how the various types of forcing are introduced in the model, three main subjects will be discussed. First, some observed and modeled current data will be shown in order to verify the capability of the model to reproduce observational data with an acceptable accuracy when reproducing barotropic currents (section 3.1) and thermohaline fields (section 3.2). Then a new current pattern will be described in the Ría de Vigo from simulations with typical forcing in the study area (section 3.3), showing a more complex behavior than that specified by a typical two-dimensional (2-D) estuarine density gradient circulation pattern [Pritchard, 1955] usually applied to the Rías Baixas [Fraga, 1981]. Finally, a discussion about the importance of remote wind forcing in the subtidal circulation of the ria is developed.

2. Data Set and HAMSOM Model

2.1. Data Set

[6] Two AANDERAA Doppler Current Meters (DCM12) were deployed in the Ría de Vigo in 1997 (Figure 1). One was deployed in the sill of the northern mouth of the ria, at a depth of 25 m, during three different periods in exactly the same position (in the deployment an iron and cement structure was used to protect the DCM12 which also ensured the exact location of the point), the first one in spring, from 10 April 1997 to 16 May 1997, the second one in summer, from 2 July 1997 to 9 September 1997, and the third one in autumn, from 9 September 1997 to 24 October 1997. Although the second and third moorings are consecutive with only a small time gap in between them, they are treated as different moorings because different AANDERAA DCM12 current meters were used. The other DCM12 was deployed in the southern mouth of the ria (Figure 1) at a depth of 45 m, but the recording period was only for 10 days from 6 to 16 October 1997.

[7] The AANDERAA DCM12 is an acoustic current meter that uses Doppler effect to measure marine currents. It sends sound pulses of a determined frequency, then receives the echo from suspension particles, and then esti-

mates the water velocity from the frequency shift between the sent and received sound waves. The AANDERAA DCM12 divides the water column into five layers (which partially overlap) with centers uniformly distributed in the water column (in this case at approximately 3.5, 7, 11, 14, and 18 m). The depth-averaged velocity for each layer, roughly 6 m thick, is then registered. The DCM12 also has a pressure sensor that allows measuring the sea surface height and hence tidal height. The time interval at which each sample was taken was set to 10 min for the first deployment and 30 min for the second and third deployments, thus allowing a high time resolution in any of them.

[8] Overlapping totally or partially in time with the moorings of current meters, 10 conductivity-temperature-depth (CTD) campaigns were made covering five different periods in the year. At each of these campaigns, measurements with a SEABIRD 25 Sealogger CTD were made in 11 different stations distributed all over the channel of the ria (Figure 1). The set of 11 stations was occupied in 6–7 hours and the order of station sampling was always opposite to the tide flow. The sampling strategy adopted was, obviously, an effort to reduce the effect of the tide, since at the Ría de Vigo the most important harmonics are the semidiurnal ones. The CTD configuration used in the campaigns allowed a sampling frequency of 4 Hz. Since the CTD was lowered at a speed of 1 m s^{-1} , the profile vertical resolution was about four samplings per meter. After the standard processing steps (and visual inspection of each profile) recommended by Sea-Bird Electronics Inc. [Sea-Bird Electronics Inc., 2000], the thermohaline data were inverse distance interpolated (with a correction factor in the vertical coordinate equal to the ratio: length of the ria to mean depth, thus avoiding a vertical homogenization) in order to obtain the thermohaline contours.

[9] Different data sets from the Instituto Nacional de Meteorología (INM) (Spanish Institute of Meteorology) of Spain were chosen to introduce the forcing in the model. Wind data set (Figure 2) from Cape Fisterra meteorological station (Figure 1); temperature, rainfall, and relative humidity from the Bouzas meteorological station; and rainfall and cloudiness from Peinador meteorological station (Figure 1).

2.2. HAMSOM Model

[10] The model used in this work is a C++ recoded version of the FORTRAN HAMSOM model, originally developed by the Institut für Meereskunde Hamburg and the Programa de Clima Marítimo (PCM) of Puertos del Estado (Spain) [Backhaus, 1983, 1985; Backhaus and Hainbucher, 1987; Rodríguez and Alvarez, 1991; Rodríguez *et al.*, 1991; Stronach *et al.*, 1993]. The C++ code is more compact than its FORTRAN counterpart, with approximately half the number of code lines, more efficient from a computational point of view, requiring less time to run a given simulation, and allows an easier introduction of new code with the implementation of C++ classes. A typical run with 50,000 calculation points, which allows cells of $300 \times 300 \text{ m}$ and 16 levels, takes 5 min d^{-1} of simulation in an Athlon 800 MHz personal computer.

[11] The HAMSOM model is a 3-D multilevel (z coordinate) finite difference baroclinic model. The starting point

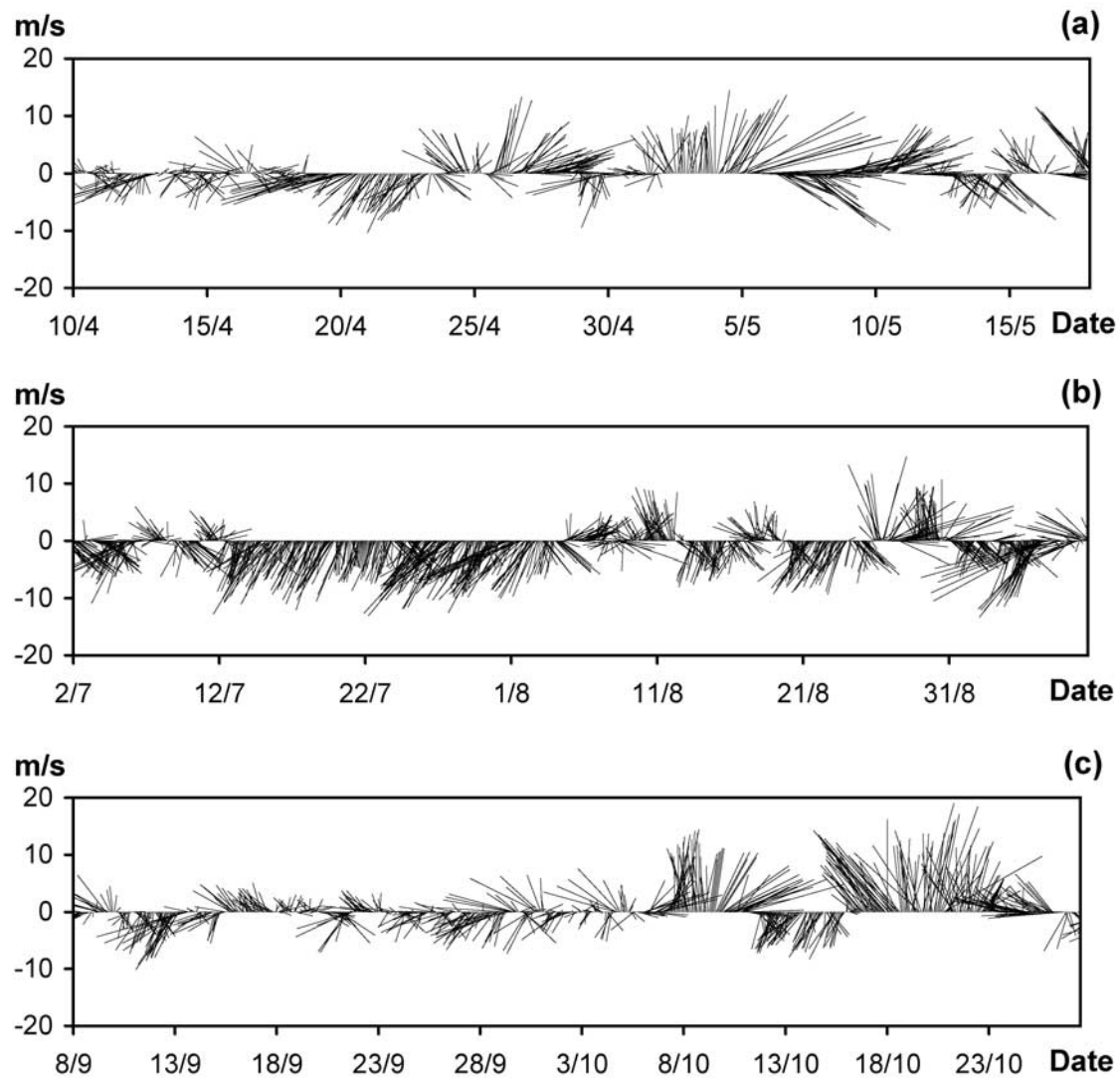


Figure 2. Wind data set from the meteorological station located at Fisterra Cape (Figure 1) for (a) spring, (b) summer, and (c) autumn.

for HAMSOM is the Navier-Stokes equations, the mass conservation equation, and the advection diffusion equations for salt and temperature. HAMSOM uses three fundamental hypotheses [Alvarez *et al.*, 1997]: (1) the hydrostatic approximation, which limits the use of the model to the simulation of long period waves, such as tidal waves or Tsunamis; (2) the assumption that seawater is an incompressible fluid, thus avoiding the simulation of sound waves; and (3) the Boussinesq approximation, taking into account the density changes of the fluid only in its floatability and not in its inertia.

[12] The equations are discretized using an Arakawa-C grid and a two time-level numerical scheme [Alvarez *et al.*, 1997], in which some terms (like pressure gradient or vertical diffusive stress) are dealt with semi-implicitly and others (momentum advection and horizontal diffusion) explicitly. The model runs with 13 layers, with centers at 2, 5, 8, 12, 17, 25, 35, 45, 55, 65, 75, 85, and 95 m under the surface. This allows a suitable degree of vertical resolution at special points like the Rande Strait or the northern mouth. The time step was set to 120 s, small

enough to guarantee stability according to the Courant-Friedrichs-Levy criterion.

2.3. Boundary Conditions

[13] The bathymetry used as impermeable boundary condition (the normal component of the velocity is null at the bottom) was obtained from charts of the Spanish Naval Hydrographic Institute and discretized to a grid of square cells with 300×300 m. The oceanic western side of the modeled domain was placed at a longitude of -9° (Figure 1). This limit was selected so that a major part of the total volume of the grid is placed over the shelf, thus allowing upwelling and downwelling inside the ria without much influence of the finiteness of the volume of integration. The northern border was placed at $42^\circ 21'N$ so that the influence on the northern mouth by the presence of the nearby island Onza is taken into account. The southern border was placed at $42^\circ 5'N$ and the eastern one at the Rande Strait, where the bottom rises sharply along 2 km, from a maximum depth of 20 m up to very shallow waters with a depth of about 3 m. A zero-gradient condition was

also imposed for the velocity in order to weaken further the discontinuity disturbances at these open boundaries. At first the thermohaline boundary condition at these vertical borders was also set as the zero gradient one. After the HAMSON results with only wind forcing (see section 3.1) were obtained and the influence of upwelling-downwelling events was stated, a more appropriated open boundary condition was imposed at the western border of the domain (section 3.2).

[14] The surface forcing includes the precipitation measured at Bouzas meteorological station (Figure 1), evaporation, heat exchange with the atmosphere (radiative, sensible, and latent), and wind stress. The evaporation is parameterized as a function of surface salinity, surface temperature, atmospheric temperature, wind celerity, and relative humidity with the algorithms from *Álvarez-Salgado et al.* [2000]. The surface salinity and temperature are known from the last step of the model results and the atmospheric variables from the data set of the Bouzas meteorological station. The heat exchange is also parameterized with the set of algorithms shown by *Álvarez-Salgado et al.* [2000]. Again, the same surface temperature, surface salinity, wind celerity, atmospheric temperature, and relative humidity are needed, but this time the cloudiness from Peinador meteorological station (Figure 1) is required to calculate the solar and terrestrial irradiance. The wind forcing is introduced as a surface boundary condition imposing the wind horizontal stress vector through the equation:

$$\boldsymbol{\tau} = C_D \rho_a |\mathbf{W}| \mathbf{W}, \quad (1)$$

where $\mathbf{W} = (W_x, W_y)$ is the wind velocity near the sea surface, C_D is a dimensionless drag coefficient, and ρ_a is the air density. The coefficient C_D is selected according to Smith's criteria [*Smith*, 1980]:

$$C_D = \begin{cases} 1.1 \times 10^{-3} & |W_{10}| < 6 \text{ m s}^{-1} \\ (0.61 + 0.06|W_{10}|)10^{-3} & 6 \text{ m s}^{-1} < |W_{10}| < 22 \text{ m s}^{-1} \end{cases}.$$

[15] The most representative shelf wind data set available for the model domain is measured at the (INM) meteorological station sited at Cape Fisterra (Figure 1). These data are representative of shelf winds, but not of the winds in the inner part of the ria. To take into account this difference between external and internal winds, Fisterra wind (Figure 2) was imposed uniformly over the shelf and the external part of the ria, westward from Cape Home. And then, eastward of Cape Home, it was decreased linearly from its shelf value down to zero at Rande Strait. This extrapolation of winds was chosen for simplicity and is consistent with the observed diminishing winds, gravity waves, and roughness of the sea along the axis of the ria down to Rande Strait.

[16] At the bottom boundary a quadratic law was used to parameterize the bottom stress:

$$\mathbf{t}_b = C_b \mathbf{u}_L |\mathbf{u}_b|,$$

where \mathbf{u}_b is the horizontal velocity at the bottom level, and \mathbf{u}_L is the vertically averaged horizontal velocity in a friction

layer whose depth was set to $d = 5$ m. This avoids large jumps in the values of friction wherever the bottom level of the model is thin [*Rodríguez et al.*, 1991]. The parameter C_b includes a friction coefficient divided by the square of the depth of the friction layer: $C_b = R d^2$. The value of R was set to 0.0025 kg m^{-1} , and $d = 5$ m.

[17] The bathymetry used in the simulation has its eastern limit at Rande Strait (Figure 1). Beyond this limit San Simón Bay is found, a zone excluded from the model domain because it has an average depth of 3 m and empties to a large extent at low tide (4 m is the tidal range of spring tides in the Ría de Vigo). However, its influence must be taken into account because of the important mixing of thermohaline properties and the buffering effect generated in this region. Furthermore, salinity and temperature results obtained at Rande show an important dependence on the unavoidable errors made when discretizing the bathymetry (important in this case because of the shallowness of San Simón Bay). Thus to solve these problems, the approach explained in the following paragraphs was used to introduce the velocity, temperature, and salinity fields at this boundary.

[18] The vertical mean value of the velocity was calculated from the river discharge, which was obtained following the empirical formula of *Ríos et al.* [1992], while a zero-gradient condition at the eastern limit of the modeled area ensured the conservation of the inner vertical variation of horizontal velocities. The river temperature (T^a), when the river water reaches the San Simón Bay, was also easily obtained because we have assumed that the river temperature is proportional to the atmosphere temperature, as *Rosón et al.* [1997], *Álvarez-Salgado et al.* [2000], or *Gilcoto et al.* [2001] have done. Then the water temperature going out of San Simón Bay was estimated under the (crude) assumptions that the tidal-induced mixing in San Simón generates a vertical homogeneous and horizontal linear distribution of temperature ranging from the river temperature to the calculated one by the model at the eastern border in the last step (T_{t-1}). The new temperature (T_t) at the eastern limit is calculated following

$$T_t = T^a + \frac{(T_{t-1} - T^a)}{2} B, \quad (2)$$

where B is a constant that depends on the volume and shape (a wedge for example) assigned to San Simón Bay.

[19] Since a good correlation was found between the mean vertical values of CTD-measured salinity at the Rande CTD station (Figure 1) and the river discharge, a more direct calculus was designed for the salinity field. The freshwater inflow was calculated from the daily precipitation at the Peinador meteorological station using an empirical formula [*Ríos et al.*, 1992], then the correlation allows the direct prediction of the salinity from precipitation with an acceptable uncertainty (Figure 3). However, while the mean salinity calculated with the minimum squares lineal fit is a good approximation to the experimental values (the determination coefficient $R^2 = 0.87$), the variations predicted occur very quickly as it corresponds to the variation of river discharge due to precipitation. The salinity at Rande should have a smoother variation and occur with a larger delay than the river discharge because of the buffering effect

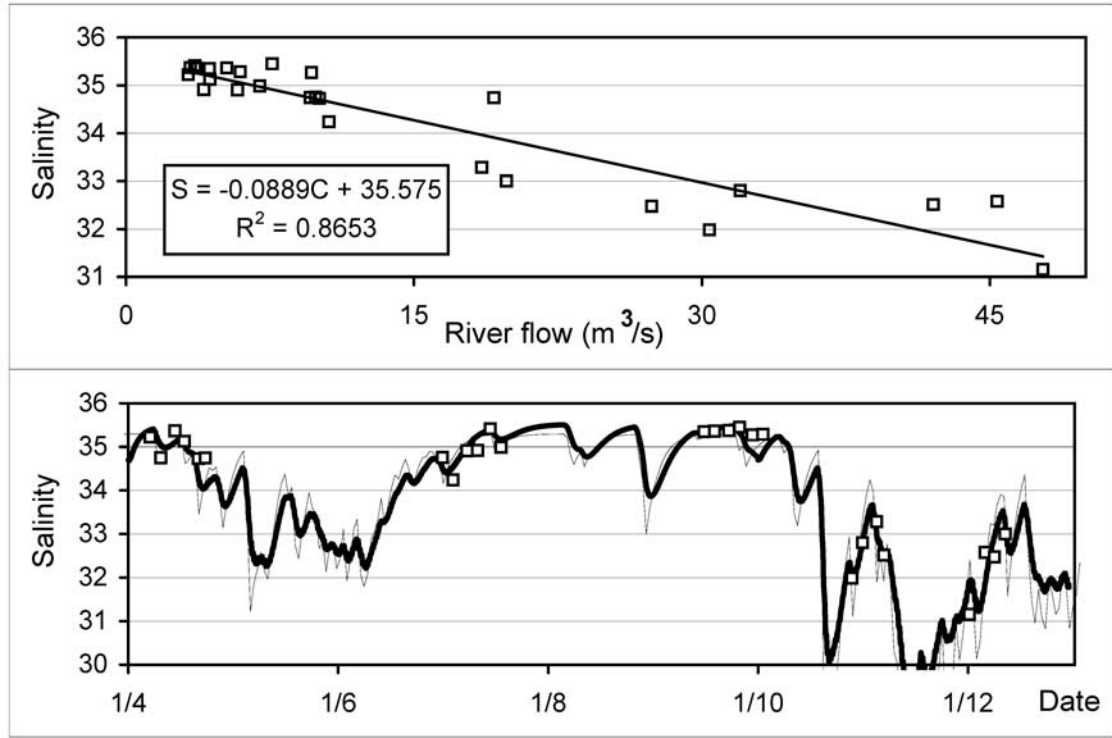


Figure 3. Minimum squares fit of salinity versus river inflow (top). The time evolution (bottom) of this minimum squares fit (thin line) compared to the Monte Carlo method (thick line) shows the smoother behavior of the latter. In both graphics, in situ salinity data from San Simón CTD station (Figure 1) are represented with an open square. The determination coefficient between in situ salinity and the Monte Carlo approximation is 0.969.

of San Simón Bay. To get more accurate values of the mean salinity at Rande, a numerical method was developed based on the approximate relation between the river discharge and the mean salinity. The formula used assumes a reduction of salinity due to the flow of freshwater in San Simón Bay. When the income of freshwater stops, the salinity will return to higher values. The formula used makes the assumption that in the case of no precipitation, salinity would asymptotically reach a determined value. So the proposed formula is:

$$S_{t+1} = S_t((V_{SS} - \Delta t C)/V_{SS}) + A(|S_R - S_t|^p)\Delta t, \quad (3)$$

where S_{t+1} is the mean salinity at Rande for the next time step, S_t is the actual salinity, the parameter A regulates the salinity augment when freshwater income falls, S_R is the reference salinity value that would be reached in the case of zero precipitation, p takes into account the quickness with which the transition takes place, depending on the difference between the actual salinity value and the reference value, V_{SS} is the known San Simón Bay volume, C is the freshwater inflow from the river, and Δt is the time step used by the model. The unknown parameters, S_R , A , and p were found with a Monte Carlo method, searching for the value which minimizes the differences between the observed salinity and the salinity predicted by formula (3). The values obtained by this method were:

$$A = 0.2456 \quad S_R = 35.80 \quad p = 1.427.$$

[20] The mean salinity at Rande determined with this method shows a smoother behavior, the standard deviation from measured salinity data (0.23) is also lower than the minimum squares one (0.35), and the determination coefficient was higher ($R^2 = 0.969$) (Figure 3). The reference value for salinity obtained by the Monte Carlo method is sensibly higher than minimum squares one, but this value is more approximated to observed values for NACW in the Atlantic margin of the region [Álvarez-Salgado *et al.*, 1993; Castro *et al.*, 1994] and also shows a good agreement with data recorded in the outer side of the ria during the 26 campaigns made.

3. HAMSOM Results

3.1. HAMSOM Barotropic Results Versus Acoustic Doppler Current Profiler Measured Currents

[21] The first step to evaluate the model's results was its validation with in situ data. A comparison of barotropic results of the model with available current data was made applying only the wind stress forcing. Thus the river inflow was set to zero (the barotropic river effect is neglected), steadiness and uniformity were assumed for the thermohaline fields and evaporation, precipitation and air sea heat exchange were not allowed. In this way it will be shown that the remote wind is usually the most important forcing agent in the Ría de Vigo [Rosón *et al.*, 1997; Álvarez-Salgado *et al.*, 2000; Souto, 2000; Souto *et al.*, 2001], extending its influence even at high (tidal) frequencies. The

Table 1. Root-Mean-Square (RMS) of the Difference (Centimeter per Second) Between Observed and Simulated Current Time Series (Figure 4) and the Corresponding Determination Coefficients (R^2)

RMS/ R^2	Spring Mooring		Summer Mooring		Autumn Mooring	
	Upper Layer	Lower Layer	Upper Layer	Lower Layer	Upper Layer	Lower Layer
Nontidal currents	7.4/0.61	10.7/0.33	7.4/0.48	8.0/0.01	5.6/0.87	7.3/0.71
Tidal currents	11.5/0.49	13.9/0.23	11.3/0.24	12.4/0.03	9.9/0.65	11.9/0.48

wind stress forcing at the sea surface was calculated through equation (1) using data from the meteorological station of the INM at Cape Fisterra. These data correspond to a place about 200 km north of the area of study, but comparison of these wind data to another station placed at Ons Island (just at the northern border of the model, data set not shown) showed that wind data are not significantly different from one place to another, all over the Rías Baixas coastline. So Fisterra data set was chosen due to its longer time coverage and also its future availability.

[22] The results shown were obtained with only one run of the model, covering the whole year of 1997. Simulated data, corresponding in the model domain to the locations of the DCM12 moorings, were recorded for all the five layers measured by the current meter. When the layer's width and position in the model do not correspond with that of the current meter, as is usually the case, interpolation between the nearest layers was calculated in order to achieve a result as similar as possible to the field data. Observed currents were quality controlled and subject to a high-frequency filter with a cutoff frequency of 1 hour [Godin, 1972]; both tidal and meteorological frequencies are therefore present in the data. Direct comparison without elimination of tidal frequencies from experimental data was preferred because the currents induced by some meteorological forcing events do achieve the frequency range of the semidiurnal tides. In order to perform quantitative nontidal comparison, a loss-pass filter with a cutoff frequency of 30 hours (A24A24A25, [Godin, 1972]) was also applied to real data, and then the root-mean-square (RMS) of the difference between the filtered in situ data and the HAMSOM results was calculated. The determination coefficient was also obtained, and the results are shown in Table 1 (this table also resumes the same statistics for the nonfiltered in situ data).

[23] At the spring mooring, the currents exhibit a relatively complex structure (Figures 4a and 4b), related to the high variability of the wind stress forcing (Figure 2a). After an initial period of little movement, some episodes of strong inflow (positive currents in Figure 4) and outflow (negative in Figure 4) currents occur (SE and NW, respectively). Sometimes the event is short in time and energetic, with strong diurnal oscillations (e.g., two outflow peaks the 24 and 26 April, diurnal inflows around 14 May), while in other cases it lasts for several days with weak high-frequency oscillations (outflow from 30 April to 5 May). Toward the end of the period (from 13 to 15 May) three diurnal peaks are observed in in situ data. Despite being a barotropic simulation, the model reproduces with an acceptable approximation the main part of the most energetic pulses of the observed currents, while the least energetic period, the first 10 days (Figures 2a, 4a, and 4b), is not modeled correctly. In addition, the modeled upper layer's

response is better suited to the observed currents (60% of the variance explained) than the lower layer's response (Table 1). Finally, it is worth noting that the outflow events associated with southerly winds (from 30 April to 5 May) seem to be better reproduced by the model than the inflow events associated with northerly winds (from 13 to 15 May).

[24] The summer period is less energetic than the spring (Figures 4c and 4d), and the barotropic model does not reproduce properly the in situ currents. In fact, this is the worst-fitted mooring, both in the upper layer and in the bottom layer (Table 1). And, although the RMS difference between simulated and observed currents is of the same magnitude as the corresponding ones for the spring mooring, the currents are lower. The determination coefficients (0.48 and 0.01 for the upper and lower layer, respectively) clearly show the mismatch. However, again, when there is an energetic pulse associated with southerly winds the barotropic model's response is adequate (11 and 27 August). And again, as a general comment, the experimental currents are better reproduced at the upper layer (Table 1).

[25] The data collected during the autumn mooring (Figures 4e and 4f) are the best modeled mooring with an 87% of the variance explained in the upper layer and with a 71% in the bottom layer (Table 1). The mooring can be divided into four periods. During the first one, from the beginning until 6 October, very low currents were recorded. Despite being a low-energy period, the model works better than in the low-energy periods of previous moorings (the RMS is the lowest in both layers as is shown in Table 1). Between 6 and 10 October, with a predominance of southerly winds, a peak of strong outflow currents appears (both in the upper and lower layers) under the influence of southerly winds, and the currents are present both in the modeled and observed data. From 10 until 17 October follows a period of northerly winds, and the corresponding currents show the same pattern in modeled and experimental data but again showing a lower magnitude in the model's results (mainly in the lower layer). After 17 October and until the end of the period, with a predominance of important southerly winds, a pattern of strong currents occurs, again well simulated by the model both in shape and magnitude as well as in the high-frequency peaks of this period.

[26] From all these comparisons, it seems that the barotropic model results agree with observed ones when the wind forcing has a mean southerly component. With northerly winds, modeled data variations sometimes are similar to current meter data but with a lower magnitude. The determination coefficients and the RMS are shown in Table 1. The spring and autumn correlations are therefore significant for the number of data collected (in all cases greater than 2000 points). During summer the correlation is evidently worse because the winds were flowing in the main part of the mooring from the north, and the wind data

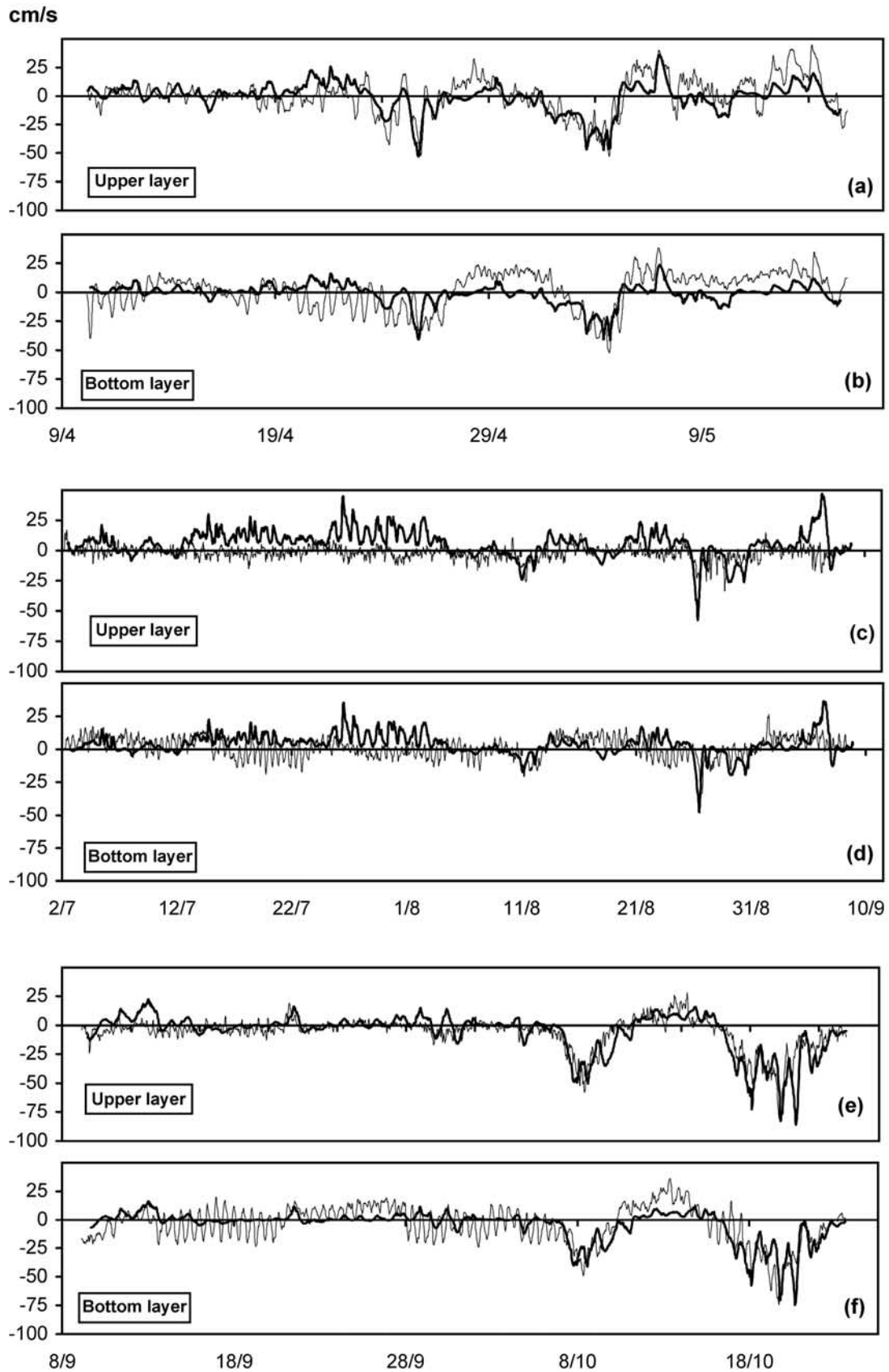


Figure 4. Current velocity component, in the main inflow-outflow direction (perpendicular to the section showed in Figure 9), at the north mouth of the Ría de Vigo for (a) and (b) spring, (c) and (d) summer, and (e) and (f) autumn periods, corresponding to the top and bottom layer of the DCM12 data (thin line) and modeled data (thick line).

set used had some gaps, which were filled with linear interpolation.

[27] Concerning the vertical variation of horizontal velocities and to get a proper view of their time evolution, the low-frequency velocity component in the main inflow and outflow direction (the directions perpendicular to the mooring sections shown in Figure 7) at each of the mooring positions was calculated (Figure 5) in order to study and compare the vertical dynamical structures of the residual circulation. The results show during a typical upwelling and downwelling situation that a two-layer circulation pattern is not developed at the northern mouth. The model reproduces this behavior and two layers are not observed in calculated data (Figure 5, top). At the southern mouth, a two-layer structure is formed during autumn, with a level of no movement that depends on the strength of wind forcing. At the beginning of the period the upper layer extends throughout almost all the water column and evolves to a two-layer circulation with a level of no movement at approximately 20 m depth, behavior that is reproduced accurately by the model (Figure 5, bottom) although the barotropic simulated currents have a lower intensity.

[28] Some important facts can be inferred from this simulation. First, the wind can explain most of the current's variability found in the northern mouth, and even some diurnal peaks are the result of wind forcing, thus showing that current's response to wind forcing is very quick, with a lag of only a few hours between the beginning of the forcing and the resulting currents. Second, the wind currents can overcome tidal currents, as can be seen from experimental data and as was also found with wind- and tide-driven simulations [Souto *et al.*, 2001]. Third, all the water column at the northern mouth moves basically in the same direction, without the formation of a two-layer structure. The intensively studied [Prego *et al.*, 1990; Prego and Fraga, 1992; Álvarez-Salgado *et al.*, 2000; Gilcoto *et al.*, 2001] two-layer circulation is maintained at the south mouth and toward the inner part of the ria.

3.2. HAMSOM Results With Baroclinic and Barotropic Forcing

[29] Once the model has been tested barotropically, next step is its validation including baroclinic forcing as well. To achieve this goal, salinity and temperature variations due to exchanges with atmosphere and river inflow (with its own thermohaline values and temporal variations, section 2.3) are introduced in the model. In the oceanic boundary of the model there is no need of an extra condition (in addition to the zero gradient one) when the currents cross this boundary toward the shelf. However, when the water comes from the shelf, two different situations can be distinguished depending on whether there is an upwelling or a downwelling situation. In the case of downwelling, the inflow into the ria occurs through the upper layer. In this case with a zero-gradient condition the model reproduces the salinity and temperature fields quite accurately. When the situation is that of upwelling, the zero-gradient condition is not good enough because it does not give the model any information about the colder and saltier water that flows toward the ria through the deeper layers. To avoid this problem a nudging condition was imposed in the western border bottom layer of the model. When the current at this depth in the model is

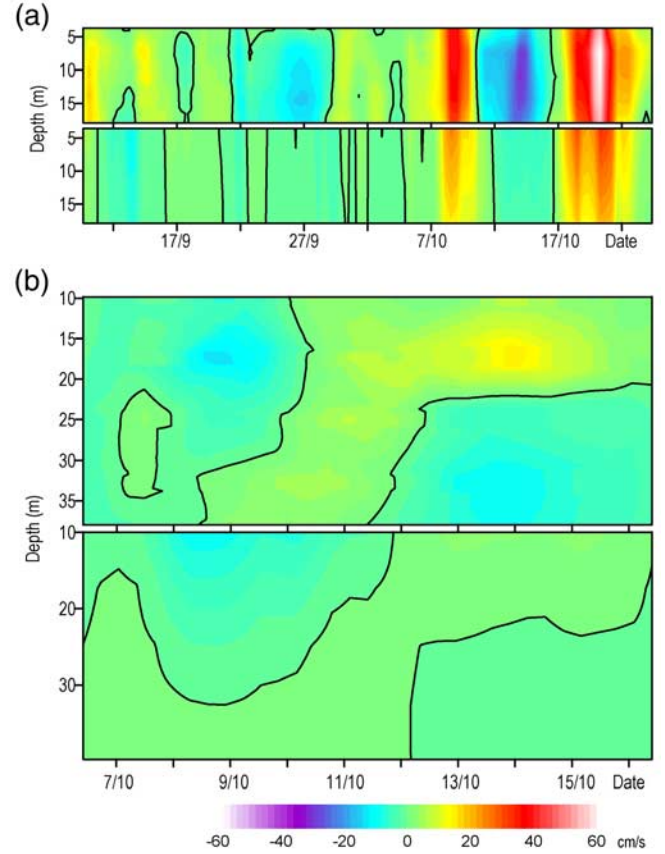
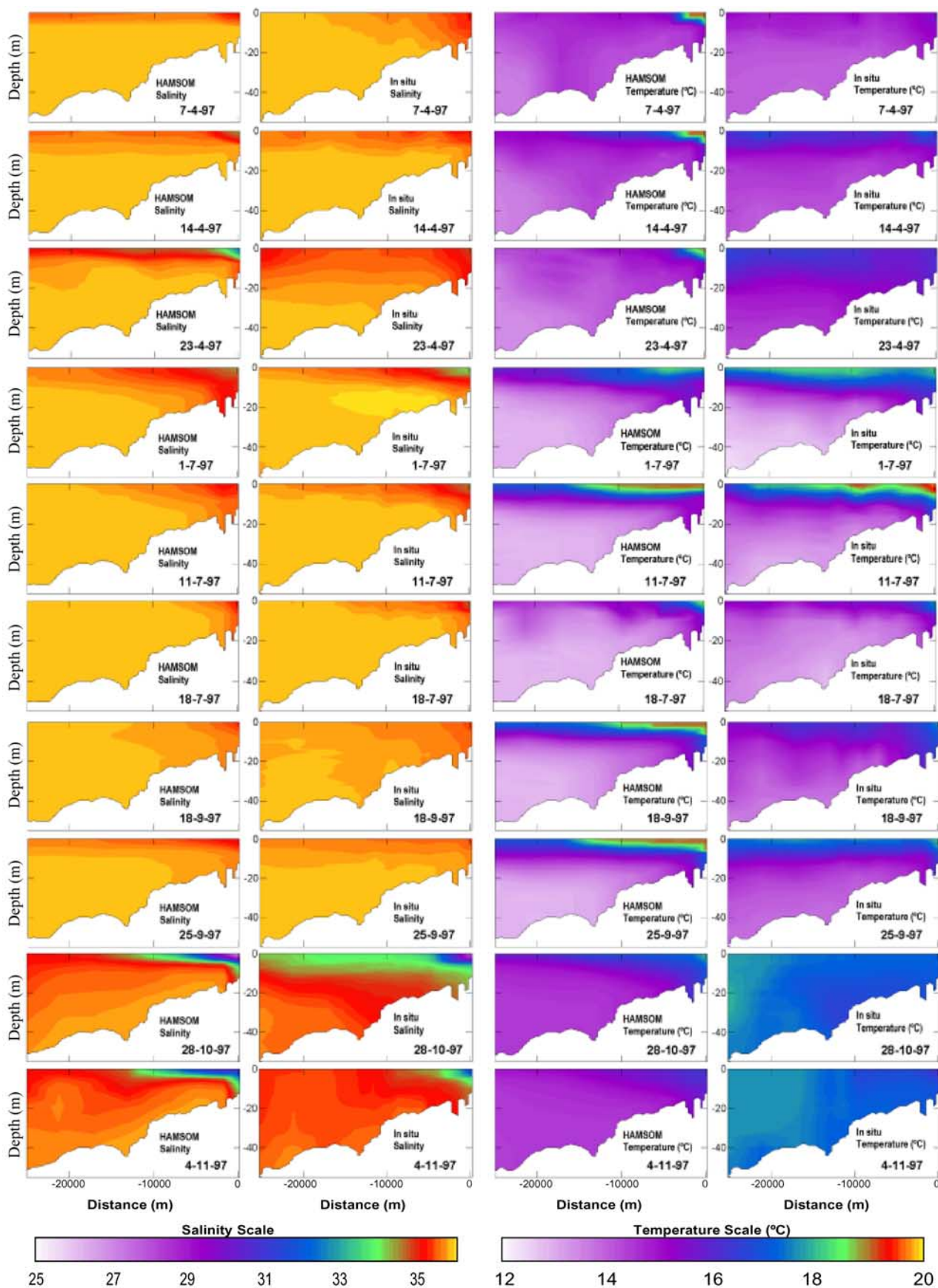


Figure 5. Time evolution of the velocity profile at the (a) north mouth and (b) south mouth. The velocity contoured is the tide-filtered horizontal component in the main direction of inflow-outflow (perpendicular to the sections showed in Figure 9) at each mooring. No double-layer circulation can be observed in either the experimental (Figure 5a, top) or in the calculated (Figure 5a, bottom) data at the north mouth. At the south mouth the model (Figure 5b, bottom) reproduces the formation of double layer during some periods of the mooring and the circulation in only one layer during other periods, as is found in observed data (Figure 5b, top).

positive (toward the ria, upwelling situation), a combination between the zero-gradient condition and a fixed-border condition was set at the corresponding border cells. In this situation, the salinity and temperature in these cells are calculated as the actual value of the fields minus the difference of this value and a reference value multiplied by the current and a constant:

$$F(t_{n+1}) = F(t_n) - (F(t_n) - F_R)ua,$$

where $F(t_{n+1})$ is the value of the field for the next time step, $F(t_n)$ is the actual value of the field, F_R is the reference value, u is the component of the velocity perpendicular to that border, and a is a constant whose value was adjusted until the calculated salinity and temperature values were similar to the observed values. This method allows simulation of an upwelling situation. If the current is large, the salinity and temperature at the border would be more



similar to the reference ones (shelf values, 12.5°C for temperature and 35.8 for salinity) as it happens in an upwelling situation.

[30] The results shown in Figure 6 for the case of baroclinic modeling were obtained with only one run of the model, starting on 1 February 1997 and finishing in December, covering all the days when data are available. The initial fields of temperature and salinity (T , S) were set to reference values of $T = 14^\circ\text{C}$ and $S = 35.8$, according to the typical values of these fields found in the ria. The relaxation time needed to reach results similar to CTD observed values all over the ria volume was estimated in 1 month. Another extra month was simulated before modeled data are compared with experimental ones, thus avoiding any further influence of the initial conditions on the results.

[31] The model is able to simulate the annual variability of the temperature and salinity fields with the exception of the October and November temperatures (Figure 6). Table 2 shows the RMS difference between CTD and HAMSOM thermohaline data, and the model seems to fit well with the measured data with the exception of the last two sampling dates. For these months (November and October), the temperature RMS is greater than the temperature range found with the CTD. The offset (about 2°C) in the autumn temperature is a consequence of the 12.5°C reference shelf temperature imposed in the oceanic boundary, too cold for the autumn season [Frouin *et al.*, 1990; Nogueira *et al.*, 1997a]. If a better thermal fitness of the model is desired in autumn, a seasonal variable reference temperature must be imposed. However, the temperature bias in autumn and winter does not introduce an important error in the baroclinic forcing (density gradients) because density in the ria during this season is mainly controlled by salinity variations (see the salinity range in Table 2).

[32] If we calculate, as a quality indicator of model results, the percentage between the RMS and the thermohaline range with the data of Table 2 (but excluding the two last campaigns that have a clear thermic bias), then the worse reproduced campaign is the one made on 23 April (41 and 62% in salinity and temperature quality index, respectively). On the other hand, the best one is that of 11 July with 22 and 16% in salinity and temperature quality index, respectively. A visual inspection of the contour plots showed in Figure 6 also corroborate that the three summer campaigns are the best reproduced by the model, both with appropriate vertical and longitudinal structures well resolved. A mismatch between the HAMSOM thermohaline fields and the CTD fields is the overestimated river runoff (head of the ria on 14 and 23 April and on 18 and 25 September) probably related with the calculation of the river runoff. We calculated the river runoff with a rainfall parameterization [Ríos *et al.*, 1992] that does not take into account that the Oitabén-Verdugo River is partially dam regulated.

[33] The thermohaline structures observed in the plots of Figure 6 seem reasonably reproduced. Besides the seasonal

Table 2. Root-Mean-Square (RMS) Differences Between the CTD-Measured Thermohaline Fields and HAMSOM Thermohaline Fields Shown in Figure 6, and Ranges of the CTD-Measured Thermohaline Fields

Date	Salinity RMS	Salinity Range	Temperature RMS, $^\circ\text{C}$	Temperature Range, $^\circ\text{C}$
<i>Spring Campaign</i>				
7 April 1997	0.21	0.70	0.76	1.68
14 April 1997	0.28	0.77	0.82	2.60
23 April 1997	0.40	0.99	1.39	2.25
<i>Summer Campaign</i>				
1 July 1997	0.52	1.88	1.41	5.77
11 July 1997	0.26	1.18	1.05	6.40
18 July 1997	0.31	1.02	1.58	4.02
<i>Autumn Campaign</i>				
18 September 1997	0.16	0.40	0.66	3.39
25 September 1997	0.16	0.48	0.89	3.95
28 October 1997	1.42	6.16	1.65	0.98
4 November 1997	1.03	2.94	2.42	1.18

variation in thermohaline fields, the model reproduces events of upwelling (18 September and 4 November), the evolution of thermohaline fields (1–18 July), and the depth of the thermocline and halocline. Although the numbers shown in Table 2 suggest that more development is necessary to achieve a quantitatively comparable response of the model, future improvements, as has been pointed above, are the correct estimates of river runoff and seasonal and short-scale time variation of reference shelf thermohaline values.

3.3. A New Circulation Pattern

[34] Once the model has been tested and validated, simulations can be made in order to determine the response of the Ría de Vigo to different wind forcings. To achieve this goal, a simple wind pattern was selected: a sinusoidal time evolution from a stationary situation of southerly winds to another of northerly winds, with a typical transition period of 4 days (Figure 7a). In order to study the response of the ria to this wind pattern, four cross-shore sections were selected, two of them in the northern and southern mouths and the other two perpendicular to the main channel and located in the inner part of the ria (Figure 7b).

[35] The results obtained once a stationary pattern has been established, after 2 days blowing southerly winds of 10 m s^{-1} , show at the southern mouth a main current pattern with a two-layer circulation (Figure 8d) inverse to the classical estuarine circulation pattern (inflow at the upper layer and outflow under 30–40 m). On the other hand, the northern mouth does not show a two-layer circulation pattern (Figure 8c). There is only a strong outflow in this mouth. The surface current penetrates the ria (Figure 8e) through the southern mouth, and in the outer part of the interior of the ria (between the Cies Islands and Cape Estai section (Figure 7b)) two branches are split: one goes ahead

Figure 6. (opposite) Matrix of modeled and in situ contour plots showing the variation of temperature (first and second columns, respectively) and salinity (third and fourth columns, respectively) along the main channel of the ria. Each plot is a vertical section following the transect depicted by the CTD stations shown in Figure 1. The distance origin of each plot is located at San Simón CTD station. Each row of the matrix of plots represents a sample date.

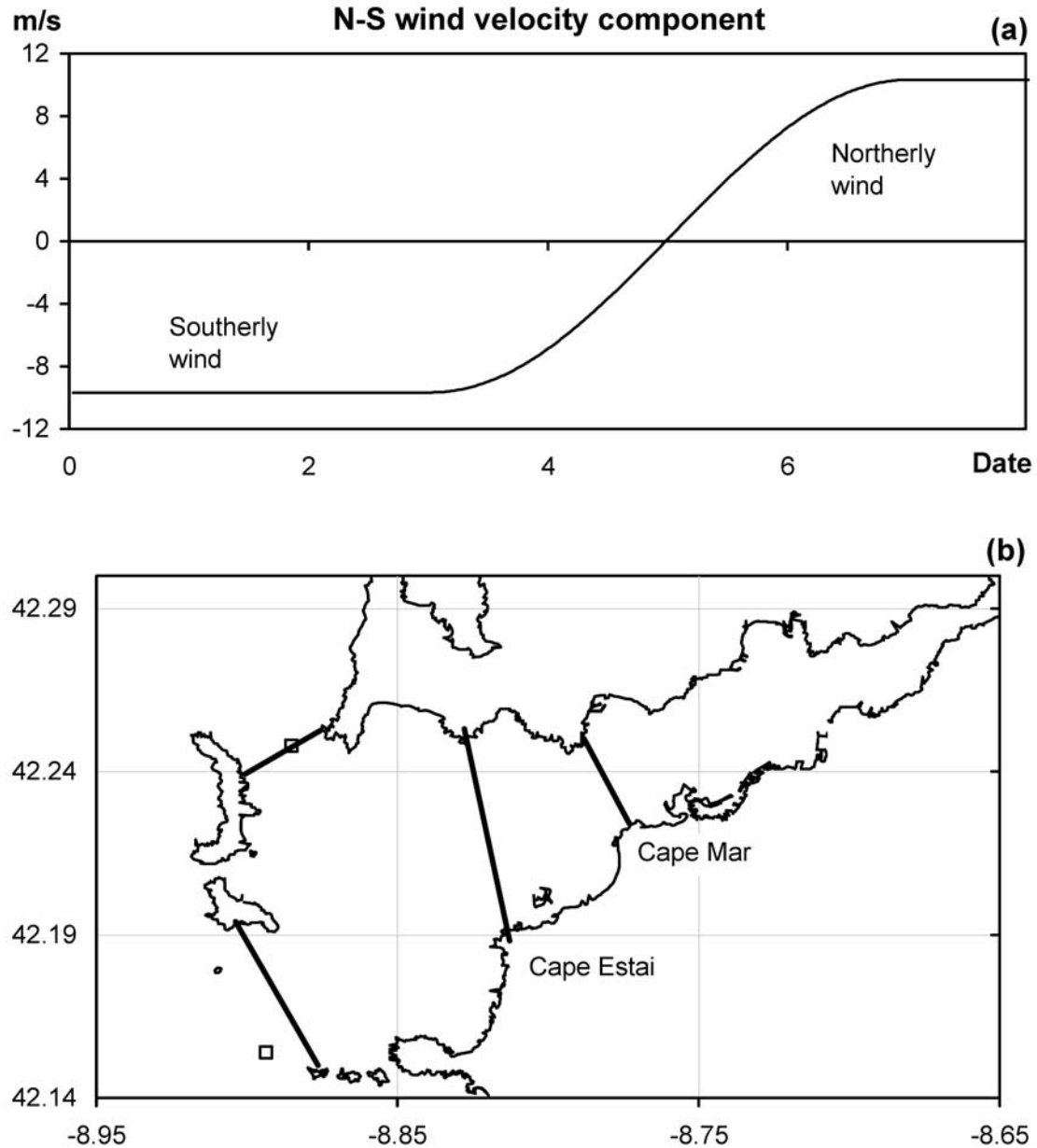
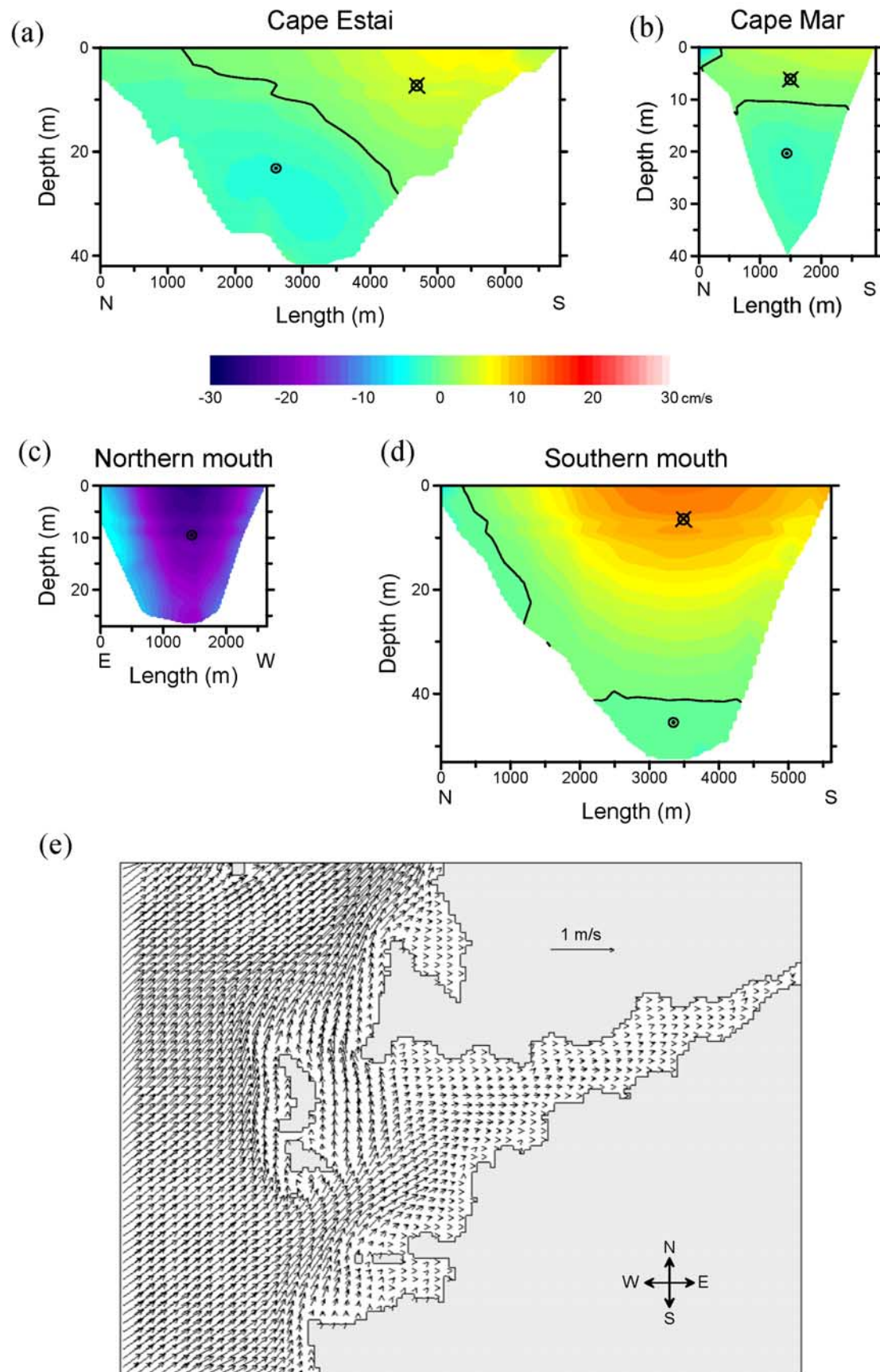


Figure 7. (a) North-south component of the wind used as input forcing for the HAMSOM simulations described in section 3.3. (b) Sections selected to determine the modeled velocity pattern at each point of the Ría de Vigo (see section 3.3 in the text).

to the head of the ria and the other turns left, northward, and finally flows out of the ria through the northern mouth. Since the northern mouth is shallower (25 m deep) than the southern mouth (55 m deep) and than the level of no motion, the velocities in this mouth are high (Figure 8c), and the flow structure at this point of the ria resembles a hydraulic jump.

[36] The former described features are generated by the interaction between the currents and the topographic configuration of the Ría de Vigo. In the middle part of the ria (between Cape Estai and Cape Mar sections) (Figure 7b), the ria narrows, and the bathymetry becomes shallower (Figure 1). So at Cape Mar section the current finds more resistance and slows down its velocity, thus feeding the

Figure 8. (opposite) Modeled residual velocity across each of the sections selected in Figure 9: (a) Cape Estai section, (b) Cape Mar section, (c) northern mouth section, and (d) southern mouth section. (e) The upper layer (from surface to 10 m depth) horizontal residual velocity field. The graphics are the result of a HAMSOM simulation with a stable southerly wind of 10 m s^{-1} .



branch that leaves the ria through the northern mouth with a strong current, and the level of no motion rises in the water column (Figure 8b). Toward the inner part of the ria, the circulation agrees with the often assumed two-layer circulation (inverse estuarine circulation in this case) with inflow at the upper layer and outflow at the bottom layer (Figure 8b). The velocities found at the cross sections from Cape Estai (Figure 8a) to Cape Mar (Figure 8b) show a horizontal variation from outflow velocities near the northern side of the ria to inflow velocities in the southern one. Thus in the ria southerly winds produce an inflow at the upper layer deflected to the south due to the influence of the southern mouth (over four times bigger than the northern mouth).

[37] Four days after this situation, when the wind forcing changes to northerly winds (Figure 7a), the current pattern also changes, with a time lag of 2 hours with respect to the wind forcing, showing a behavior opposite to the one driven by southerly winds. This time the vertical flow structure in the southern mouth (Figure 9d) is the classical two-layer estuarine circulation (outflow in the surface layer and inflow in the bottom layer), and the northern mouth presents, again, a strong velocity in the whole water column although with opposite sense (Figure 9c): the current is entering in the ria through the northern mouth and the bottom layer of the southern mouth and leaving the ria through the surface layer of the southern mouth. Toward the inner part of the embayment, the two-layer circulation pattern persists (Figure 9b), with an outflow at the upper layer and an inflow at the bottom layer. The surface velocity field (Figure 9e) gives us a good picture to describe the circulation scheme generated by upwelling winds: the surface current in the inner part of the ria is flowing to the southern mouth and, in the outer part of the ria, this current receives the water flux that enters in the ria through the northern mouth and flows southward.

[38] The simplified circulation scheme of a downwelling situation in the Ría de Vigo is depicted in Figure 10. The upwelling situation would show a similar scheme but with all the arrows pointing in the opposite sense. In fact, the scheme could be divided into two parts: (1) a classical 2-D estuarine circulation pattern applied to the inner part of the ria, and (2) a more complex 3-D scheme applied to the outer part of the ria.

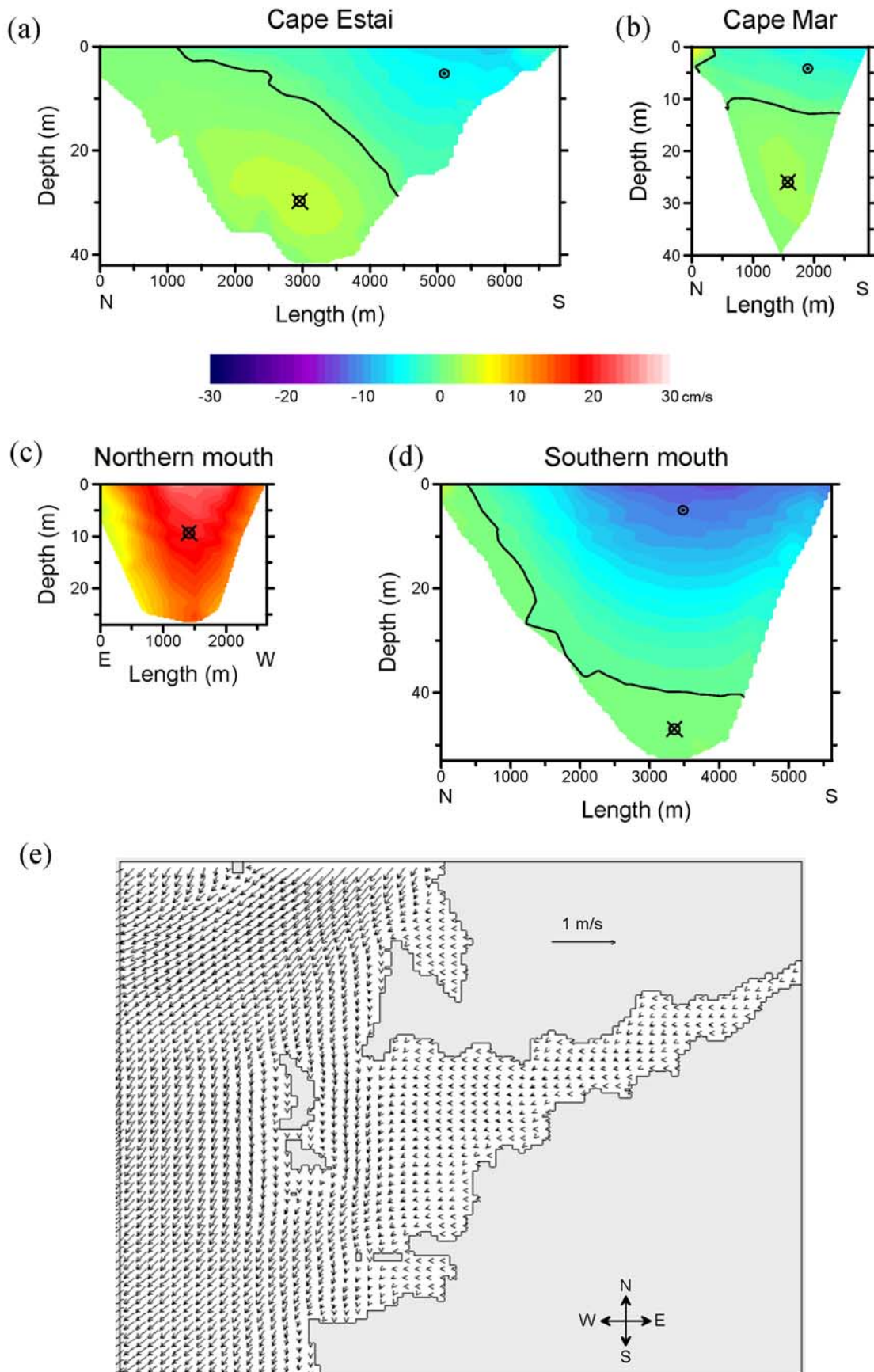
[39] We can link the simplified residual circulation scheme proposed for the Ría de Vigo in Figure 10 with the mechanism responsible for it taking into account that the upwelling/downwelling events are 3-D processes [Smith, 1983]. This is observed in Figures 8e and 9e, which show that the residual surface currents beyond the Cies Islands have an important component in the alongshore direction (alongshore jet), i.e., in an upwelling (downwelling) situation the surface water is moving offshore (onshore) because of the Ekman transport but also southward (northward) because of the direct action of the wind drag and the geostrophic adjustment derived from the sea level gradients generated by the cross-shore Ekman transport (in an

upwelling/downwelling the sea level near coast is lower/higher than the sea level in the shelf) [Csanady, 1982; Smith, 1983]. So besides the 2-D vision of a two-layer estuarine circulation enhanced by the offshore Ekman transport of an upwelling event suggested by authors as Rosón *et al.* [1997], there is a 3-D one. In the 3-D scheme of residual circulation forced by remote wind, which we have observed and described, the alongshore jet associated with upwelling or downwelling events and its interaction with the topographic features of the Ría de Vigo (two mouths generated by the presence of the Cies Islands and the funnel shape of the ria) have a key role. Thus in an upwelling situation the alongshore jet is southward and enters in the ria through the northern mouth and leaves the ria through the southern mouth (Figure 9e). On the other hand, in a downwelling situation the alongshore jet is northward and enters the ria through the southern mouth and leaves the ria through the northern mouth (Figure 8e).

4. Discussion

[40] More than 20 years ago, Carter *et al.* [1979] pointed out the importance of remote forcing of nontidal variability in water level and motion in estuaries had been reached in the U.S. research. In the Galician coasts the nonlocal influence of upwelling in the interior of the rias has been internationally recognized since the article of Fraga [1981]. Moreover, the upwelling shelf processes in the region were studied several times [Fiúza, 1983; Blanton *et al.*, 1984; McClain *et al.*, 1986] in 1980s since Wooster *et al.* [1976] had written about the upwelling cycle along the eastern boundary of the North Atlantic. In addition, the upwelling and the well-known seasonal hydrographic patterns [Nogueira *et al.*, 1997a, 1997b] in the Rías Baixas and Galician shelf [Álvarez-Salgado *et al.*, 1993; Castro *et al.*, 1994] have been driving the evolution of the box models applied to this area. The first box models applied to the rias [Prego *et al.*, 1990; Prego and Fraga, 1992] rapidly became obsolete because they were salt balance and stationary box models that were only able to reflect the imposed river quasi-stationary residual circulation (not the river flood pulses only the long-term average river flow). Its stationary condition impeded the correct estimation of the nonstationary by nature upwelling/downwelling events and their interaction with the river buoyancy forcing at scales around 4–5 days. Also, its salt balance dependence mislead the summer model results because in this season the salinity vertical gradient is lower than the numerical stability required by the model. As Álvarez-Salgado *et al.* [2000] and Gilcoto *et al.* [2001] have explained clearly, such problems were successfully worked out by Rosón *et al.* [1997] with the aid of a nonstationary- and thermohaline-weighted box model. Thus the nonstationary character of the Rosón *et al.*'s model has enhanced the time response of the box models applied to the Rías Baixas allowing short timescale (4–5 days) thermohaline and meteorological

Figure 9. (opposite) Modeled residual velocity across each of the sections selected in Figure 9: (a) Cape Estai section, (b) Cape Mar section, (c) northern mouth section, and (d) southern mouth section. (e) The upper layer (from surface to 10 m depth) horizontal residual velocity field. The graphics are the result of a HAMSOM simulation with a stable northerly wind of 10 m s^{-1} .



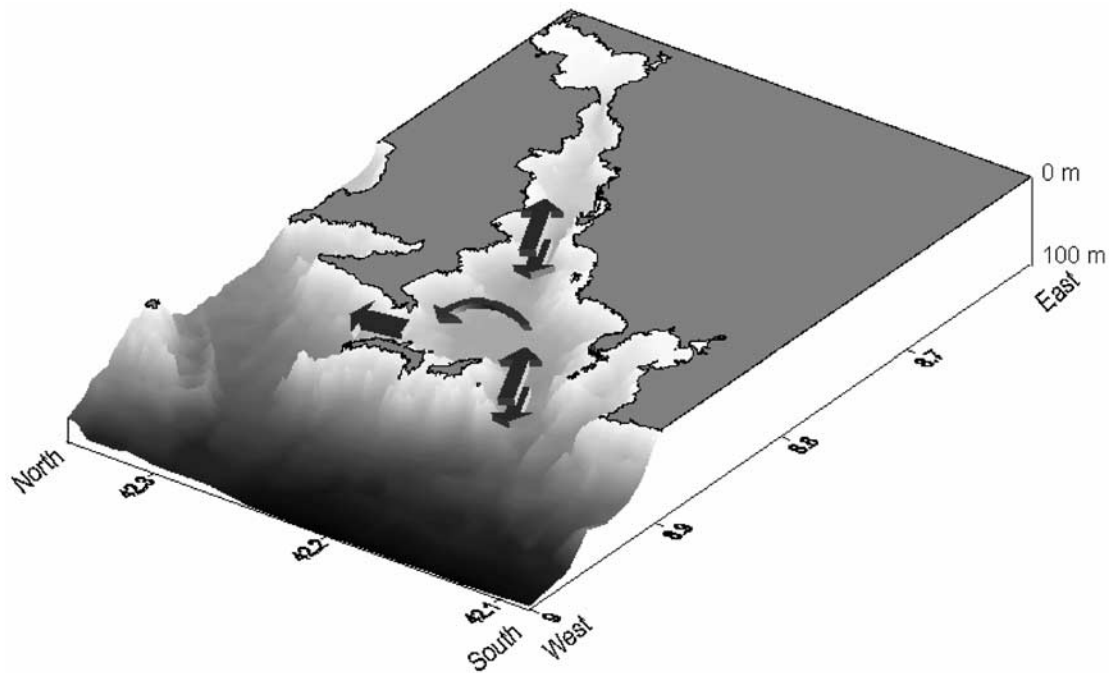


Figure 10. Scheme of the new pattern found at the Ría de Vigo. Extensively studied double-layer circulation combines with a north-south circulation at the outer part of the ria, maintaining the typical pattern for partially mixed estuaries at the inner side.

coupling studies [Pardo *et al.*, 2001] and its thermohaline-weighted algorithm has greatly improved the robustness of the box model solutions.

[41] Although the tidal-induced residual current theories [Ianniello, 1977, 1979; Prandle and Rahman, 1980; Prandle, 1982; Aubrey, 1985; Speer, 1985] have not been rigorously applied to the Rías Baixas, nor the ebb-flood asymmetry [Jay and Smith, 1990a; Peters, 1997], nor the spring-neap transitions [Simpson *et al.*, 1990; Jay and Smith, 1990b] and despite that the Ría de Vigo is a mesotidal and semidiurnal ($F = 0.095$) estuary, tidal characteristics that may enhance the former nonlinear processes, the Ría de Vigo response to upwelling is surprisingly efficient and many times overcome tidal or river residual currents (sections 3.1 and 3.3). The link between upwelling and the ria's residual circulation was first quantified on the basis of simple 2-D box models in the 4–5 day timescale context. Now with the aid of the validated HAMSOM model with current meter data, this assertion is corroborated, and the timescale response of the Ría de Vigo to meteorological forcing has been shown to reduce even to events of diurnal periods. Moreover, since there were no significant differences in the estimation of currents among only wind forced HAMSOM results (section 3.1) and baroclinic HAMSOM results (section 3.2), one may conclude that wind forcing must be always included in simulations with the purpose of obtaining reliable and realistic results with a numerical model. This has been considered by some authors [Souto, 2000; Souto *et al.*, 2001; Torres López *et al.*, 2001] but not by others [Taboada *et al.*, 1998; Gómez-Gesteira *et al.*, 1999]. Obviously, this does not mean that the nonlinear tidal processes, river flood events, stratification processes, etc. could be forgotten when a ria is modeled or studied. In fact, we have not included the tidal forcing as an input in the HAMSOM model, and

the tidal frequencies have not been filtered out in the current meter data, because one of the aims of this article is to show the importance that the wind forcing has on the circulation of the ria.

[42] The new circulation pattern presented in section 3.3 must be taken as one of the most probable residual circulation pattern in the Ría de Vigo many times along the course of a year. Not only because the modeled results shown here agree with in situ data but also because the pattern is consistent with the alongshore jet associated to upwelling/downwelling situations [Csanady, 1982] flowing in the shelf and close to the coast. Thus when an upwelling (downwelling) event occurs the corresponding alongshore jet is southward (northward) directed and could penetrate in the ria crossing it from north (south) to south (north). Indeed, since the length of the Ría de Vigo is small in comparison with the wavelength associated with the upwelling events the theory developed by Garvine [1985] suggests that the remote wind forcing must be important in the ria. Garvine [1985] developed a simple theoretical model to illustrate the physical foundations of the low-frequency fluctuations (5–20 days) forced by remote wind in Chesapeake Bay and the subtidal fluctuations in the Delaware Estuary. Prior to Garvine [1985], Klinck *et al.* [1981] were able to generalize the fjordlike estuaries' response to remote forcing with a two-layer, linear, frictionless model of the coupled shelf/estuary circulation, and Bakun *et al.* [1984] suggest that this model will reproduce the circulation in the Rías Baixas quite well. On the other hand, Walters [1982] found sea level fluctuations in South Bay (San Francisco Bay) with a period of 7 hours that were coherent with nonlocal wind forcing. He argued that the higher frequency response in comparison with that found in Chesapeake Bay is a consequence of the smaller size of

San Francisco Bay as compared to Chesapeake Bay. So it is not surprising that the smallest Ría de Vigo presents diurnal current fluctuations due to remote wind forcing. Thus if the estuarine residual currents and all the processes and interactions driving such currents are studied from a nonstationary point of view [Jay and Flinchem, 1997; Jay and Flinchem, 1999] then the wind-induced residual current pattern presented here must be taken as the most frequent one but not as the only one possible nor as a stationary one.

5. Conclusions

[43] The 3-D finite difference HAMSOM model has been adapted to the Ría de Vigo (NW Spain) and tested both barotropically and baroclinically, applying the forcing of wind, freshwater input from rivers and all over the surface, and heat interchange with atmosphere. A new method has been developed to calculate the salinity at the eastern boundary of the model once the river runoff is known, using a Monte Carlo algorithm to adjust the corresponding parameters. The Monte Carlo method allows the prediction of the salinity at this border, and the parameters found are in good agreement with corresponding experimental values. A nudging method to set the western (oceanic) boundary conditions without diminishing the model-predictive capacity was also developed and applied.

[44] The results obtained with the model have been compared with both DCM12 current data and CTD salinity and temperature data along the main channel. The modeled results are shown to be in agreement with experimental data in both cases. The model reproduces the most important events that happened during the current meter moorings, both in temporal duration and amplitude, nevertheless with a diminishing of amplitude with northerly winds. For the baroclinic simulations, the model appears to be capable of simulating the annual variability of the salinity and temperature fields as well as some events of upwelling and downwelling. During some periods, the temperature field shows a pattern that indicates the existence of convection cells along the main channel of the Ría, thus allowing an upward velocity in one place of the channel combining at the same time with downward velocity in another place. Finally, both modeled results and experimental current meter data have shown the importance of upwelling events in the residual currents of the Ría de Vigo, i.e., the great influence that wind forcing has in the modulation of the residual currents since the Ría de Vigo is located in the northern boundary of the Iberian Peninsula, just at the NW of the Africa upwelling system.

[45] Finally, the agreement between the HAMSOM simulations with the in situ data also allows us to infer and propose a new 3-D residual circulation pattern in the outer part of the Ría de Vigo based on HAMSOM results (section 3.3). The results have been obtained after we had run the model with a typical wind forcing time series (Figure 7a) that begins with a downwelling, continues with a transition period, and ends with an upwelling.

[46] **Acknowledgments.** The authors are grateful to the crew of the oceanographic vessel *Mytilus* for their unconditional help. We would like to thank X. A. Álvarez-Salgado for useful comments on the manuscript. Comments by two anonymous reviewers are very much appreciated. This

work was supported by CICYT Project AMB95-1084 and FEUGA Project "Ordenación integral do espacio marítimo-terrestre de Galicia."

References

- Álvarez, E., B. Pérez, and I. Rodríguez, A description of the tides in the Eastern North Atlantic, *Prog. Oceanogr.*, 40, 217–244, 1997.
- Álvarez-Salgado, X. A., G. Rosón, F. F. Pérez, and Y. Pazos, Hydrographic variability off the Rías Baixas (NW Spain) during the upwelling season, *J. Geophys. Res.*, 98, 14,447–14,455, 1993.
- Álvarez-Salgado, X. A., J. Gago, B. M. Miguez, M. Gilcoto, and F. F. Pérez, Surface waters of the NW Iberian margin: Upwelling on the shelf versus outwelling of upwelled waters from the Rías Baixas, *Estuarine Coastal Shelf Sci.*, 51, 821–837, 2000.
- Backhaus, J. O., A semi-implicit scheme for the shallow water equations for application to shelf sea modeling, *Cont. Shelf Res.*, 2(4), 243–254, 1983.
- Backhaus, J. O., A three-dimensional model for simulation of shelf sea dynamics, *Dtsch. Hydrogr. Zeitschrift*, 38(H.4), 165–187, 1985.
- Backhaus, J. O., and D. Hainbucher, A finite difference general circulation model for shelf seas and its application to low frequency variability on the North European Shelf, in *Three-Dimensional Models of Marine and Estuarine Dynamics*, Elsevier Oceanogr. Ser., vol. 45, edited by J. C. J. Nihoul and B. M. Jamart, pp. 221–244, Elsevier Sci., New York, 1987.
- Bakun, A., and C. S. Nelson, The seasonal cycle of wind-stress curl in subtropical eastern boundary current regions, *J. Phys. Oceanogr.*, 21, 1815–1834, 1991.
- Blanton, J. O., L. P. Atkinson, F. Fernández de Castillejo, and A. Lavín, Coastal upwelling off the Rías Baixas, Galicia, northwest Spain, I, Hydrographic studies, *Rapp. P. V. Reun. Cons. Int. Explor. Mer.*, 183, 79–90, 1984.
- Blanton, J. O., K. R. Tenore, F. Castillejo, L. P. Atkinson, F. B. Schwing, and A. Lavín, The relationship of upwelling to mussel production in the rias on the western coast of Spain, *J. Mar. Res.*, 45, 497–511, 1987.
- Carter, H. H., T. O. Najarian, D. W. Pritchard, and R. Wilson, The dynamics of motion in estuaries and other coastal water bodies, *Rev. Geophys.*, 17(7), 1585–1590, 1979.
- Castro, C. G., F. F. Pérez, X. A. Álvarez-Salgado, G. Rosón, and A. F. Ríos, Hydrographic conditions associated with the relaxation of an upwelling event off the Galician coast (NW Spain), *J. Geophys. Res.*, 99, 5135–5147, 1994.
- Cotton, C. A., Rias sensu stricto and sensu lato, *Geogr. J.*, 122, 360–364, 1956.
- Csanady, G. T., *Circulation in the Coastal Ocean*, 279 pp., D. Reidel, Norwell, Mass., 1982.
- Dyer, K. R., *Estuaries: A Physical Introduction*, 195 pp., John Wiley, New York, 1997.
- Fiúza, A. F. G., Upwelling patterns of Portugal, in *Coastal Upwelling: Its Sediment Record*, edited by E. Suess and J. Thiede, pp. 85–97, Plenum, New York, 1983.
- Flinchem, E. P., and D. A. Jay, An introduction to wavelet transform tidal analysis methods, *Estuarine Coastal Shelf Sci.*, 51, 177–200, 2000.
- Fraga, F., Upwelling off the Galician coast, northwest Spain, in *Coastal Upwelling*, vol. 1, *Coastal and Estuarine Science*, edited by F. A. Richards, pp. 176–182, AGU, Washington, D. C., 1981.
- Fraga, F., and R. Margalef, Las rías gallegas, in *Estudio y explotación del mar en Galicia*, pp. 101–121, Santiago de Compostela, 1979.
- Frouin, R., A. Fiúza, I. Ambar, and T. J. Boyd, Observations of a poleward surface current off the coasts of Portugal and Spain during winter, *J. Geophys. Res.*, 95, 679–691, 1990.
- Garvine, R. W., A simple model of estuarine subtidal fluctuations forced by local and remote wind stress, *J. Geophys. Res.*, 90, 11,945–11,948, 1985.
- Garvine, R. W., R. K. McCarthy, and K.-C. Wong, The axial salinity distribution in the Delaware estuary and its weak response to river discharge, *Estuarine Coastal Shelf Sci.*, 35, 157–165, 1992.
- Gilcoto, M., X. A. Álvarez-Salgado, and F. F. Pérez, Computing optimum estuarine residual fluxes with a multiparameter inverse model method (OERFIM): Application to the Ría de Vigo (NW Spain), *J. Geophys. Res.*, 106, 31,303–31,318, 2001.
- Gómez-Gesteira, M., P. Montero, R. Prego, J. J. Taboada, P. Leita, M. Ruiz-Villarreal, R. Neves, and V. Pérez-Villar, A two-dimensional particle tracking model for pollution dispersion in A Coruña and Vigo Rías (NW Spain), *Oceanol. Acta*, 22(2), 167–177, 1999.
- Haynes, R., and E. D. Barton, A poleward flow along the Atlantic coast of the Iberian Peninsula, *J. Geophys. Res.*, 95, 11,425–11,441, 1990.
- Haynes, R., and E. D. Barton, Lagrangian observations in the Iberian coastal transition zone, *J. Geophys. Res.*, 96, 14,731–14,741, 1991.
- Ianniello, J. P., Tidally induced residual currents in estuaries of constant breath and depth, *J. Mar. Res.*, 35, 755–774, 1977.
- Ianniello, J. P., Tidally induced residual currents in estuaries of variable breath and depth, *J. Phys. Oceanogr.*, 9, 962–974, 1979.

- Jay, D. A., Green's law revisited: Tidal long-wave propagation in channels with strong topography, *J. Geophys. Res.*, **96**, 20,585–20,598, 1991.
- Jay, D. A., and E. P. Flinchem, Interaction of fluctuating river flow with a barotropic tide: A demonstration of wavelet tidal analysis methods, *J. Geophys. Res.*, **102**, 5705–5720, 1997.
- Jay, D. A., and E. P. Flinchem, A comparison of methods for analysis of tidal records containing multi-scale non-tidal background energy, *Cont. Shelf Res.*, **19**, 1695–1732, 1999.
- Jay, D. A., and J. D. Smith, Residual circulation in shallow estuaries, 2, Weakly stratified and partially mixed, narrow estuaries, *J. Geophys. Res.*, **95**, 733–748, 1990a.
- Jay, D. A., and J. D. Smith, Circulation, density and neap-spring transitions in the Columbia River estuary, *Prog. Oceanogr.*, **25**, 81–112, 1990b.
- Klinck, J. M., J. J. O'Brien, and H. Svendsen, A simple model of fjord and coastal circulation interaction, *J. Phys. Oceanogr.*, **11**, 1612–1626, 1981.
- Li, C., and J. O'Donnell, Tidally driven residual circulation in shallow estuaries with lateral depth variation, *J. Geophys. Res.*, **102**, 27,915–27,929, 1997.
- Li, C., and A. Valle-Levinson, A two dimensional analytic tidal model for a narrow estuary of arbitrary lateral depth variation: The intratidal motion, *J. Geophys. Res.*, **104**, 23,525–23,543, 1999.
- MacCready, P., Estuarine adjustment to changes in river flow and tidal mixing, *J. Phys. Oceanogr.*, **29**, 708–726, 1998.
- Masse, A. K., Withdrawal of shelf water into an estuary: A barotropic model, *J. Geophys. Res.*, **95**, 16,085–16,096, 1990.
- McClain, C. R., S.-Y. Chao, L. P. Atkinson, J. O. Blanton, and F. F. de Castillejo, Wind-driven upwelling in the vicinity of Cape Finisterre, Spain, *J. Geophys. Res.*, **91**, 8470–8486, 1986.
- Nogueira, E., F. F. Pérez, and A. F. Ríos, Seasonal patterns and long-term trends in an estuarine upwelling ecosystem (Ría de Vigo, NW Spain), *Estuarine Coastal Shelf Sci.*, **44**, 285–300, 1997a.
- Nogueira, E., F. F. Pérez, and A. F. Ríos, Modelling thermohaline properties in an estuarine upwelling ecosystem (Ría de Vigo: NW Spain) using Box-Jenkins transfer function models, *Estuarine Coastal Shelf Sci.*, **44**, 685–700, 1997b.
- Pardo, P. C., M. Gilcoto, and F. F. Fiz, Short-time scale coupling between thermohaline and meteorological forcing in the Ría de Pontevedra, *Sci. Mar.*, **65**, suppl. 1, 229–240, 2001.
- Peters, H., Observations of stratified turbulent mixing in an estuary: Neap-to-spring variations during high river flow, *Estuarine Coastal Shelf Sci.*, **45**, 69–88, 1997.
- Prandle, D., The vertical structure of tidal currents and other oscillatory flows, *Cont. Shelf Res.*, **1**(1), 190–207, 1982.
- Prandle, D., and M. Rahman, Tidal response in estuaries, *J. Phys. Oceanogr.*, **10**, 1552–1573, 1980.
- Prego, R., General aspects of carbon biogeochemistry in the Ría de Vigo, northwestern Spain, *Geochim. Cosmochim. Acta*, **57**, 2041–2052, 1993.
- Prego, R., and F. Fraga, A simple model to calculate the residual flows in a Spanish Ría. Hydrographic consequences in the Ría of Vigo, *Estuarine Coastal Shelf Sci.*, **34**, 603–615, 1992.
- Prego, R., F. Fraga, and A. F. Ríos, Water interchange between the Ría de Vigo and the coastal shelf, *Sci. Mar.*, **54**(1), 95–100, 1990.
- Pritchard, D. W., A study of the salt balance in a coastal plain estuary, *J. Mar. Res.*, **13**, 133–144, 1954.
- Pritchard, D. W., Estuarine circulation patterns, *J. Mar. Res.*, **81**, 1–11, 1955.
- Rattray, M., and D. W. Hansen, A similarity solution for circulation in an estuary, *J. Mar. Res.*, **20**, 121–133, 1962.
- Ríos, A., M. Nombela, F. F. Pérez, G. Rosón, and F. Fraga, Calculation of runoff to an estuary: Ría de Vigo, *Sci. Mar.*, **56**(1), 29–33, 1992.
- Rodi, W., *Turbulence Models and their Application in Hydraulics: A State of the Art Review*, 104 pp., A. A. Balkema, Brookfield, Vt., 1993.
- Rodríguez, I., and E. Alvarez, Modelo Tridimensional de Corrientes: Condiciones de aplicación a las costas españolas y análisis de resultados para el caso de un esquema de mallas anidadas, *Clim. Mar. Rep.*, **42**, 65 pp., 1991.
- Rodríguez, I., E. Alvarez, J. Krohn, and J. O. Backhaus, A mid-scale tidal analysis of waters around the north-western corner of the Iberian Peninsula, in *Proceedings of Computer Modelling in Ocean Engineering*, vol. 91, 568 pp., A. A. Balkema, Brookfield, Vt., 1991.
- Rosón, G., X. A. Alvarez-Salgado, and F. F. Pérez, A non stationary box model to determine residual fluxes in a partially mixed estuary, based on both thermohaline properties: Application to the Ría de Arousa (NW Spain), *Estuarine Coastal Shelf Sci.*, **44**, 249–262, 1997.
- Sea-Bird Electronics Inc., *CTD Data Acquisition Software, Seasoft V4.244 Manual*, 149 pp., Sea-Bird Electr. Inc., Bellevue, Wash., 2000.
- Simpson, J. H., Physical processes in the ROFI regime, *J. Mar. Syst.*, **12**(1–4), 311–323, 1997.
- Simpson, J. H., J. Brown, J. B. L. Matthews, and G. L. Allen, Tidal straining, density currents, and stirring in the control of estuarine stratification, *Estuaries*, **13**(2), 125–132, 1990.
- Smith, R. L., Circulation patterns in upwelling regimes, in *Coastal Upwelling*, edited by E. Suess and J. Thiede, pp. 13–35, Plenum, New York, 1983.
- Smith, S. D., Wind stress and heat flux over the ocean in gale force winds, *J. Phys. Oceanogr.*, **10**, 709–726, 1980.
- Souto, C., Predicción numérica y contraste experimental de la circulación en la Ría de Vigo, Ph.D. dissertation, 178 pp., Univ. of Vigo, Vigo, Spain, 2000.
- Souto, C., L. Fariña, E. Alvarez, and I. Rodríguez, Wind and tide current prediction using a 3D finite difference model in the Ría de Vigo (NW Spain), *Sci. Mar.*, **65**, suppl. 1, 269–276, 2001.
- Stacey, M. T., S. G. Monismith, and J. R. Burau, Observations of turbulence in a partially stratified estuary, *J. Phys. Oceanogr.*, **29**, 1950–1970, 1999.
- Stronach, J. A., J. O. Backhaus, and T. S. Murty, An update on the numerical simulation of oceanographic processes in the waters between Vancouver Island and the mainland: The GF8 model, *Oceanogr. Mar. Biol.*, **31**, 1–86, 1993.
- Taboada, J. J., R. Prego, M. Ruiz-Villarreal, M. Gomez-Gesteira, P. Montero, A. P. Santos, and V. Perez-Villar, Evaluation of the seasonal variations in the residual circulation in the Ría of Vigo (NW Spain) by means of a 3D baroclinic model, *Estuarine Coastal Shelf Sci.*, **47**, 661–670, 1998.
- Torres López, S., R. A. Varela, and E. Delhez, Residual circulation and thermohaline distribution of the Ría de Vigo: A 3-D hydrodynamical model, *Sci. Mar.*, **65**, Suppl. 1, 277–289, 2001.
- Vives, F., and F. Fraga, Producción básica en la Ría de Vigo, *Invest. Pesquera (Barcelona)*, **19**, 129–137, 1961.
- Wais, R., On the relation of linear stability and the representation of Coriolis terms in the numerical solution of the shallow water equation, doctoral thesis, Hamburg Univ., Hamburg, Germany, 1985.
- Walters, R. A., Low-frequency variations in sea level and currents in South Francisco Bay, *J. Phys. Oceanogr.*, **12**, 658–668, 1982.
- Wong, K.-C., and J. E. Moses-Hall, On the relative importance of the remote and local wind effects to the subtidal variability in a coastal plain estuary, *J. Geophys. Res.*, **103**, 18,393–18,404, 1998.
- Wooster, W. S., A. Bakun, and D. R. McClain, The seasonal upwelling cycle along the eastern boundary of the North Atlantic, *J. Mar. Res.*, **34**, 131–141, 1976.

L. Fariña-Busto and C. Souto, Departamento de Física Aplicada, Facultad de Ciencias, Universidad de Vigo, Marcosende-Lagoas s/n, E-36200 Vigo, Spain. (ctorres@uvigo.es)

M. Gilcoto and F. F. Pérez, Instituto de Investigaciones Mariñas, Eduardo Cabello s/n, E-36208 Vigo, Spain.